Variations in carbon burial and sediment accretion along a tidal creek in a Florida salt marsh

Jill M. Arriola [1]*, **Jaye E. Cable** [1,2]
[1]Department of Marine Sciences, University of North Carolina at Chapel Hill, Chapel Hill, North Carolina
[2]Curriculum in Environment and Ecology, University of North Carolina at Chapel Hill, Chapel Hill, North Carolina

Abstract

Salt marshes store large quantities of carbon in the form of buried organic matter (OM) and consequently play a major role in the global carbon cycle, yet vertical accretion and carbon burial rates (CBRs) can vary by orders of magnitude on small spatial scales. The goal of this study was to provide insight into carbon burial variability of a single tidal salt marsh. Six marsh sediment cores were collected along a tidal creek in the Big Bend of Florida from the mouth to the coastal forest within the marsh levee and plain. Each was analyzed for porosity, % OM, total organic carbon (TOC), total nitrogen (TN), $\delta^{13}C$, $\delta^{15}N$, and excess ^{210}Pb to determine vertical accretion and CBRs. Porosity, % OM, and TOC and TN were found to be highest in the low marsh and within the marsh levee. Stable isotopes of OM indicate the source is dominated by C3 plant species in both the levee and plain. Average vertical accretion ranges from 0.9 mm yr^{-1} to 2.2 mm yr^{-1} with the slowest rates in the low marsh. Average carbon burial ranges from 49.5 g OC m^{-2} yr^{-1} to 109.5 g OC m^{-2} yr^{-1}. High carbon burial associated with low sediment accumulation in the Low Marsh and low carbon burial associated with high sediment accumulation rates in the High Marsh are typical in this marsh. These variations imply that the highest carbon burial occurs in the zone most vulnerable to loss via inundation and erosion.

The year 2013 was a landmark year for the global atmospheric carbon dioxide (CO_2) concentration in which the Mauna Loa Observatory, Hawaii, recorded the first daily mean average high of over 400 ppm (Bala 2013). Carbon dioxide is a well-known greenhouse gas responsible for the rising of global atmospheric temperature and investigations have now concluded that CO_2 is also decreasing the pH of the ocean due to partial pressure diffusion of CO_2 at the air–sea interface (Doney et al. 2009). As atmospheric CO_2 concentrations continue to rise, the warming atmosphere will lead to warming oceans, reducing the solubility of CO_2 in the oceans, causing a positive feedback of increasing atmospheric CO_2 concentrations (Houghton 2003). Mitigation of atmospheric CO_2 through sequestration and storage of carbon has been suggested as a means to preserve a stable and habitable greenhouse effect and reduce further ocean acidification (Houghton 2003).

*Correspondence: arriola@email.unc.edu

Additional Supporting Information may be found in the online version of this article.

Special Issue: Headwaters to Oceans: Ecological and Biogeochemical Contrasts Across the Aquatic Continuum
Edited by: Marguerite Xenopoulos, John A. Downing, M. Dileep Kumar, Susanne Menden-Deuer, and Maren Voss

However, coherent and consistent terminology is essential when discussing the processes involved in CO_2 mitigation for stake-holders to understand carbon management strategies. Carbon sequestration, burial, and storage are terms often used interchangeably in scientific literature. The IPCC defines carbon sequestration, also referred to as uptake, as the addition of carbon containing substances to a particular reservoir (IPCC 2014). For the purposes of this paper, this definition is interpreted to include all processes that remove CO_2 from the atmosphere, such as photosynthesis by macrophytes. Carbon burial is the process whereby the sequestered carbon is placed into storage within sediments in the top centimeters (Bost 2016). And finally, carbon storage is here defined as the state where the buried carbon is no longer exchanged with the atmosphere. However, stored sediment carbon may not be permanent as processes such as subsidence and erosion may alter these storage sites from carbon sinks to sources (Chmura 2013).

Tidal salt marshes are expected to bury vast amounts of carbon per unit area. The annual estimate of global tidal marsh carbon burial is between 0.01 Gt C and 0.09 Gt C, but the total global area of salt marshes is poorly known and the area that is known is disappearing at a rate of 0.7–7% per year (Hopkinson et al. 2012). The estimated range of annual tidal fresh and salt marsh carbon burial potential based upon

studies from across the globe is 18–1713 g C m^{-2} (Chmura et al. 2003). This wide range of carbon burial potential exists due to the variability among several factors, such as marsh vegetation type, sediment sources, and tidal ranges (Callaway et al. 2012). Local, small scale variations, such as vegetation density and geomorphology, further impact the quality and quantity of carbon burial.

Implications for carbon stored in marsh sediments becomes a question of ecosystem vulnerability in the face of changing climatic impacts, i.e., sea-level rise (SLR), subsidence, magnitude of storm surges, and increased frequency and intensity of storms. Salt marshes may migrate landward, if upland space for lateral growth is available, when threatened by SLR at the land–sea interface, resulting in a conversion of coastal forests to tidal wetlands, which may destroy potential carbon storage sites and may enhance the organic matter (OM) release to the ocean (Craft 2012). However, Morris et al. (2002) suggested that a rise in relative sea level may increase marsh vegetation productivity and biomass density, enhancing sedimentation, as the marsh makes an effort to reach equilibrium with sea level. Marshes are stable when soil surface elevation increases at a rate similar to local SLR (Morris et al. 2016). If vertical marsh accretion outpaces relative SLR, then the carbon storage potential in that marsh will increase (McLeod et al. 2011).

As SLR occurs, our understanding of carbon burial and storage in a transitioning salt marsh will be challenged. One possible approach to understanding this new paradigm is to investigate an environment where the marsh to forest succession is already underway. Tree hammocks are relics of the coastal forest that survived on topographic highs as the salt marsh migrated landward due to historic SLR (Williams et al. 1999). Marsh carbon observations including tree hammocks could be utilized to further understand the transition from terrestrial to marine vegetation and the impact of tidal inundation on carbon storage. Marsh soils contain a greater % of fine-grained sediments and higher OM content at lower elevations than those at higher elevations (Kruczynski et al. 1978). Also, tides deposit sediments along the marsh edge of tidal creeks, creating an elevated levee between the creek and the surrounding marsh plain (Meanley 1965) which can result in meter scale carbon burial variability. Here, we illustrate the spatial variability of sediment accretion and carbon burial rates (CBRs) within various stages of marsh development, from low to high marsh and from marsh levee to marsh plain, within a Florida salt marsh and determine its adaptability to SLR.

Study site

Salt marshes located along the Big Bend region of northwestern Florida represent 41% of the state's total marsh area (Montague and Odum 1997) and have been the focus of previous studies (Kruczynski et al. 1978; Coultas 1980; Cahoon et al. 1995; Choi et al. 2001) due to the relative lack of coastal development and large adjacent forested landscape. Direct human disturbances are generally confined to recreational fishing and boating. Nestled in Taylor County, Florida, between the Aucilla and Econfina rivers, resides a 20 km^2 salt marsh that adjoins the Econfina River State Park and Aucilla Wildlife Management Forest to the south and east, and is further protected by the St. Marks Wildlife Refuge and Econfina Conservation Area to the north and west. Snipe Creek, a 2.3 km long tidal creek near the center of the Aucilla-Econfina marsh, begins at the edge of the cedar and pine scrub forest and empties into the Gulf of Mexico (GoM) at the marsh edge (Fig. 1a).

The vegetation species in the salt marsh is dominated by black needle rush (*Juncus roemerianus*), covering an area about 71% throughout the interior of the marsh, followed by smooth cordgrass (*Spartina alterniflora*) covering 18% area found mainly along the creek banks and on small channel islands (D. Seminara and J. Schalles pers. comm.). The Aucilla-Econfina marsh is dotted with tree hammocks, with the largest and closest hammock to the GoM in this system located approximately 1.7 km upstream along the south bank of Snipe Creek. Plant composition on the hammock is similar to the inland coastal forest which is dominated by cedar, pine, and saw and cabbage palm trees, as well as dense underbrush.

Maximum tidal range is about 1 m at Cedar Key (Fig. 1a, NOAA station ID: 8727520), approximately 140 km SW of Snipe Creek mouth (tidesandcurrents.noaa.gov, accessed 25 October 2016). The tides at Snipe Creek are mixed semidiurnal with highs ranging from 0.5 m to 1.3 m above mean sea level. The average marsh elevation surrounding Snipe Creek is between 0.5 m and 0.75 m above mean sea level (2007 FDEM Lidar: Taylor County, csc.noaa.gov, accessed 04 June 2012). The marsh has a slope of 0.4 m km^{-1} and abuts a broad shallow, inner continental shelf (Montague and Odum 1997). Sandy marsh sediments comprise a thin 1–2 m layer which overlay the Oligocene-aged Suwannee Limestone Formation (Coultas and Gross 1975), ancient sand dune ridges (Montague and Odum 1997), and the unconfined Floridian Aquifer (Grubbs 1998). The annual mean precipitation is 150 cm (climatecenter.fsu.edu, accessed 25 October 2016) in this subtropical region, with an annual mean evapotranspiration of 110 cm (fl.water.usgs.gov, accessed 25 October 2016).

Materials

Field sampling

Two sediment cores were retrieved from three sites along Snipe Creek, totaling six cores. The sites are labeled Low Marsh, Hammock, and High Marsh, which relate to their position along the estuary (Fig. 1b). The Low Marsh cores were collected at the mouth (M) and lower mid-creek (MC),

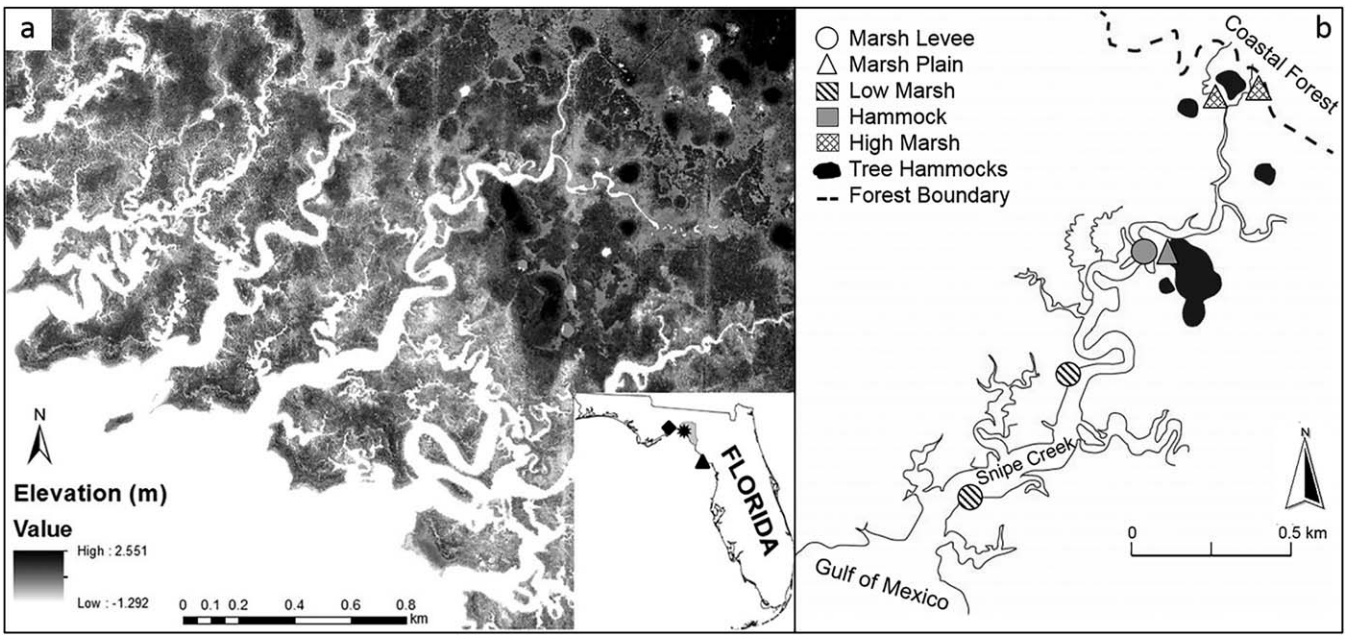

Fig. 1. (**a**) Geographical DEM representation of Snipe Creek (closed star) located in Taylor County, FL (inset). NOAA station in Cedar Key (closed triangle) and St. Marks National Wildlife Refuge (closed diamond; inset). (**b**) Locations of sample sites along Snipe Creek. Mouth (M) and MC reside within the Low Marsh levee; HE, and Interior (HI) stations consist of marsh levee and marsh plain sites; Upstream (S) and near Forest (F) are located within the High Marsh plain.

about 0.3 km and 0.8 km upstream from the creek entrance, respectively. Hammock marsh cores were collected at interior (HI) and exterior (HE) marsh locations about 1.7 km upstream from the creek entrance. The High Marsh cores were obtained from upstream creek (S) and near forest (F) locations within the salt marsh, about 2.5 km and 2.7 km upstream from the creek entrance, respectively. Sediment cores were collected from the Low Marsh site and the exterior Hammock station 12 April 2011–13 April 2011, about 1 m inland of the creek bank and within the marsh levee. The interior Hammock station and High Marsh site cores were extracted on 26 May 2013, between 10 m and 70 m from the creek bank within the marsh plain. Sediments were extracted using a polycarbonate push core (7 cm ID × 50 cm L) with beveled edges pushed into the marsh surface. Sediment heights inside and outside the coring tube were noted prior to removing the core from the sediment to estimate compaction, which is assumed to be consistent throughout the entire core. The core lengths recovered from the marsh ranged from 34 cm to 41 cm, were sectioned in 1–2 cm intervals at Econfina River State Park the day of collection, and stored cold until laboratory analysis could be conducted at the University of North Carolina, Chapel Hill, North Carolina.

Laboratory analysis

Known sample volumes were weighed damp and placed into a drying oven at 60°C for at least 48 h to ensure thorough evaporation of water content. To calculate the dry bulk density, the mass of the dry solid was divided by the known sample volume (Dingman 2002). Porosity (Φ) of the samples was calculated using the fraction of water present in the sediments (W_D), the dry bulk density (ρ_{dry}), and the density of the fluid (ρ_w) based on in situ pore water salinity measurements (Eq. 1; Corbett et al. 2000).

$$\Phi = (W_D/\rho_w)/\left[(W_D/\rho_w) + \left(1 - W_D/\rho_{dry}\right)\right] \quad (1)$$

Bulk plant material, such as root mats and rhizomes, was removed after the samples dried. The dried sediment was then homogenized using a mortar and pestle and subsamples were set aside for further analysis. For percent OM, sediments were processed via loss on ignition. Between 0.5 g and 4.0 g of sediment was distributed into pre-weighed porcelain crucibles and ignited in a Lindberg Blue M1100 muffle furnace at 550°C for 4 h to obtain percent OM content.

A 1–2 g aliquot of the dried homogenized sediment was prepared for ^{210}Pb ($t_{1/2} = 22.3$ yr) analysis by gamma spectrometry. Sediment was packed into 11 × 63 mm plastic vials and sealed with epoxy resin, capped, and stored for at least 4 weeks for equilibration of ^{226}Ra with ^{222}Rn. Samples were counted for 48 h on one of two well germanium detectors for ^{210}Pb, ^{137}Cs, and ^{226}Ra (as ^{214}Pb and ^{214}Bi) (25% relative efficiency). Germanium detectors were corrected for

background activity and calibrated using IAEA-300 Baltic Sea marine sediment standards. The activity of ^{226}Ra ($t_{1/2}$ = 1620 yr) was subtracted from the total ^{210}Pb activity and decay corrected to the time of collection to calculate unsupported ^{210}Pb ($^{210}Pb_{ex}$). No clearly defined ^{137}Cs fallout peaks appeared in any of the cores; therefore, only $^{210}Pb_{ex}$ was used to date the sediment cores. We assumed that the flux of ^{210}Pb to the surface was constant, but that the rate of the sediment supply was variable because the $^{210}Pb_{ex}$ profiles do not show a monotonic decline with depth (Appleby and Oldfield 1983; Sanchez-Cabeza and Ruiz-Fernandez 2011). Therefore, after obtaining the full $^{210}Pb_{ex}$ inventory, we used the constant rate of supply model (Appleby and Oldfield 1978 and adapted by Sanchez-Cabeza and Ruiz-Fernandez 2011) for dating the sediments:

$$A_o = \Sigma \left(^{210}Pb_{ex}\right)_i \times d_i \times \rho_i \quad (2)$$

$$A_x = A_o e^{-\lambda t} \quad (3)$$

$$t = \frac{1}{\lambda} \ln \frac{A_o}{A_x} \quad (4)$$

where A_o is the total or initial inventory of $^{210}Pb_{ex}$ (Bq kg^{-1}). The inventory is derived from the sum of $^{210}Pb_{ex}$ activity from the surface to the observed depth interval multiplied by the depth of the interval in cm (d_i), and multiplied by the dry grain density in g cm^{-3} (ρ_i) of that interval (Eq. 2). A_x is the activity of $^{210}Pb_{ex}$ for a given depth interval and λ is the ^{210}Pb decay constant of 0.03114 yr^{-1} (Appleby and Oldfield 1978; Eq. 3). Equation 3 is rearranged to solve for the time (t) it took the given sediment to accumulate (Eq. 4). Dividing the depth by t, for that depth interval provides the sediment accretion rate in cm yr^{-1}. Total sediment mass accumulation rates (g m^{-2} yr^{-1}) were calculated by multiplying the dry bulk density (g cm^{-3}) by the sediment accretion rate (cm yr^{-1}) for each interval. CBRs (g OC m^{-2} yr^{-1}) were derived by multiplying the total sediment mass accumulation rate by the total organic carbon (TOC) concentration (g OC g_{sed}^{-1}) for each interval.

An additional aliquot of the original homogenized sediment was weighed into silver capsules, vapor acidified with trace metal grade HCl overnight to eliminate inorganic carbon in the sediment, and then each silver capsule sample was dried at 80°C for 1 h before being sealed. Samples were analyzed for TOC, total nitrogen (TN), δ^{13}C, and δ^{15}N by a Carlo Erba Elemental Analyzer (NC 2500) interfaced to a Finnigan Delta Plus XP stable isotope mass spectrometer at the National High Magnetic Field Laboratory at Florida State University in Tallahassee, Florida.

Results

Porosity and % OM

Porosity and % OM values are generally highest at the levee sites (Fig. 2a, Supporting Information). The porosity of the sediments ranged between 0.38 and 0.82 at the marsh levee sites with some fluctuations at the surface of the HE. Porosity in the marsh plain ranged between 0.20 and 0.49 with the highest variability at the forest station (F). Percent OM ranged between 12% and 69% within the levee sites. The OM content at all marsh plain sites ranged from 1% to 19%, with the highest % found at mid-depth of the forest station (F). Trends in % OM depth mimic those of porosity for all sites.

Carbon and nitrogen in sediments

The TOC sediment values ranged between 0.04 g OC g_{sed}^{-1} and 0.21 g OC g_{sed}^{-1} at the marsh levee sites. TOC values are an order of magnitude lower, ranging between 0.001 g OC g_{sed}^{-1} and 0.043 g OC g_{sed}^{-1}, in the plain sites. Values of sediment TN ranged between 0.004 g N g_{sed}^{-1} and 0.012 g N g_{sed}^{-1} for all marsh sites with the lowest values at the HI. TN sediment values display a linearly increasing trend with TOC for all sites (Fig. 2b, Supporting Information). A simple linear regression suggests that TN is strongly dependent on TOC for five of the six stations, but it is more correlated within the marsh plain than within the levee sites.

The δ^{13}C values of sediments in the levee ranged between −18‰ and −27‰ with the most enriched values at depth in the HE site. δ^{13}C ranged between −22‰ and −26‰ further upstream in the plain sites with the greatest variation found at HI. Interestingly, the two hammock stations, HE and HI, are only separated by ~ 70 m and have very little overlap in δ^{13}C values (Fig. 3, Supporting Information). δ^{15}N sediment values ranged between +2‰ and −0.2‰ within the levee sites and is most depleted closest to the mouth of the creek. The δ^{15}N values ranged between +1‰ and +4‰ at the marsh plain sites. δ^{15}N becomes more depleted with depth at all stations.

$^{210}Pb_{ex}$

Surface activity of $^{210}Pb_{ex}$ (Bq kg^{-1}) is highest overall at the mouth of the creek (Fig. 4). Overall, $^{210}Pb_{ex}$ activity in the plain sites (HI, S, F) is much lower than observed in the levee sites (M, MC, HE). The $^{210}Pb_{ex}$ profile at the HE core appears to be mixed and does not show a net decline with depth. No discernable decay profile occurred in the $^{210}Pb_{ex}$ activity for the HI station as it appears to be at background levels throughout the core. Therefore, both the HE and the HI stations are not included in vertical accretion or CBRs.

The $^{210}Pb_{ex}$ inventories for the mouth, MC, upstream, and forest stations are 1893.6 Bq kg^{-1}, 1053.2 Bq kg^{-1}, 429.4 Bq kg^{-1}, and 703.5 Bq kg^{-1}, respectively. The highest $^{210}Pb_{ex}$ inventory is at the mouth which is likely due to lateral transport and subsequent settling of fine particles associated with $^{210}Pb_{ex}$ from frequent tidal inundation in addition to atmospheric deposition. Activities of $^{210}Pb_{ex}$ reach background activity of the parent ^{226}Ra within the levee sites, but ^{226}Ra activities are more variable within the plain sites. In addition, ^{226}Ra activities are greater than the $^{210}Pb_{ex}$ activities at the upstream and forest stations at mass depths

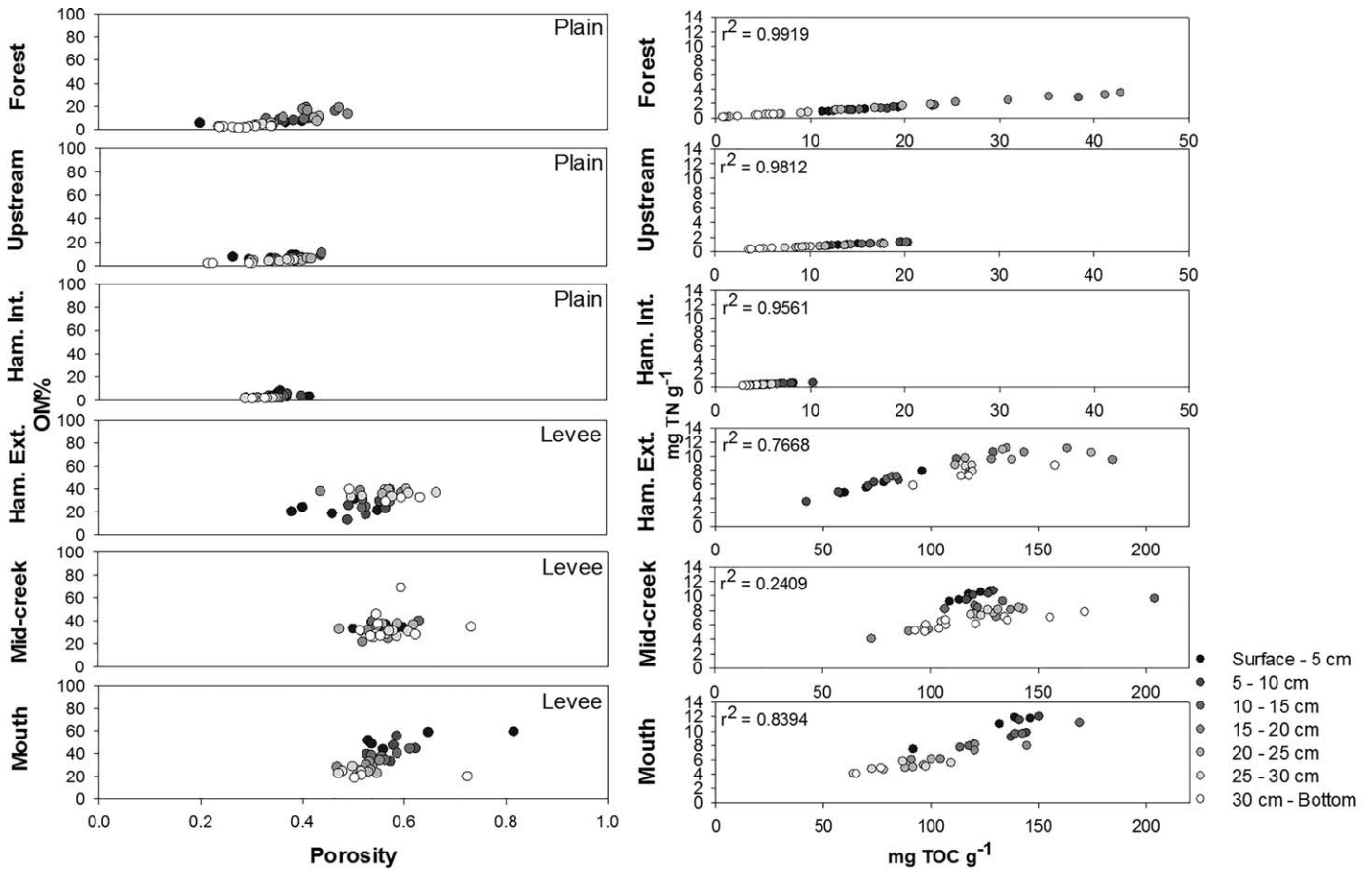

Fig. 2. (**a**) OM % vs. porosity for all stations. Depth in the core is represented by gray scale with samples at the surface denoted by black circles. Levee stations overall have higher porosities than stations located in the plain. (**b**) TN (mg TN g_{sed}^{-1}) vs. TOC (mg OC g_{sed}^{-1}) for all stations. Note: scales for TN and TOC concentrations are displayed here in mg g_{sed}^{-1}, but are listed in Supporting Information in g g_{sed}^{-1}. Also, axis labels for TOC are a larger scale for the levee stations (mouth, MC, and HE) than for the plain.

below 13 g cm^{-2} (Fig. 4). Previous studies have shown that groundwater discharge along the extent of the nearby Suwanee River, about 70 km east of Snipe Creek, is an important source of radium to the GoM (Burnett et al. 1990). The increase in ^{226}Ra at the upstream and forest stations could be derived from similar groundwater sources that carry a high radium signal due to uranium in the aquifer. This may enhance the presence of total ^{210}Pb in the sediments, but $^{210}Pb_{ex}$ is reported to account for radium sources.

Average vertical accretion rates (VARs) for the periods of record at the mouth, MC, upstream, and near forest stations are 1.5 mm yr^{-1}, 0.9 mm yr^{-1}, 2.2 mm yr^{-1}, and 2.0 mm yr^{-1}, respectively. The average accretion rate along Snipe Creek is 1.65 mm yr^{-1}. Average total sediment mass accumulation rates for the mouth, MC, upstream, and forest stations are 820.9 g m^{-2} yr^{-1}, 777.6 g m^{-2} yr^{-1}, 3245.7 g m^{-2} yr^{-1}, and 3563.1 g m^{-2} yr^{-1}, respectively. The Low Marsh overall has the lowest mass accretion rates (MARs) for this system, with the lowest rate at the mouth, which is due to deposition of finer particles and high porosities. There is an apparent increase in mass accumulation moving from the Low Marsh up to the forest (Fig. 5). Average CBRs for the mouth, MC, upstream, and forest stations are 109.5 g C m^{-2} yr^{-1}, 95.7 g C m^{-2} yr^{-1}, 49.5 g C m^{-2} yr^{-1}, and 65.2 g C m^{-2} yr^{-1}, respectively. The CBRs do not exhibit any trend from the Low to High Marsh, but the highest CBRs occur at the mouth station (Fig. 6).

Mean values of the results for each station are provided in Table 1.

Discussion

Marsh levee vs. marsh plain

Samples for the HI and High Marsh were all retrieved within the marsh plain. These inland sites are only fully inundated by spring high tides or storm events, whereas the sediments in the Low Marsh and HE, located within the marsh levee area, are frequently inundated by the typical semi-diurnal tide. The low porosity of sediments within the High Marsh could be due to changes in the type and amount

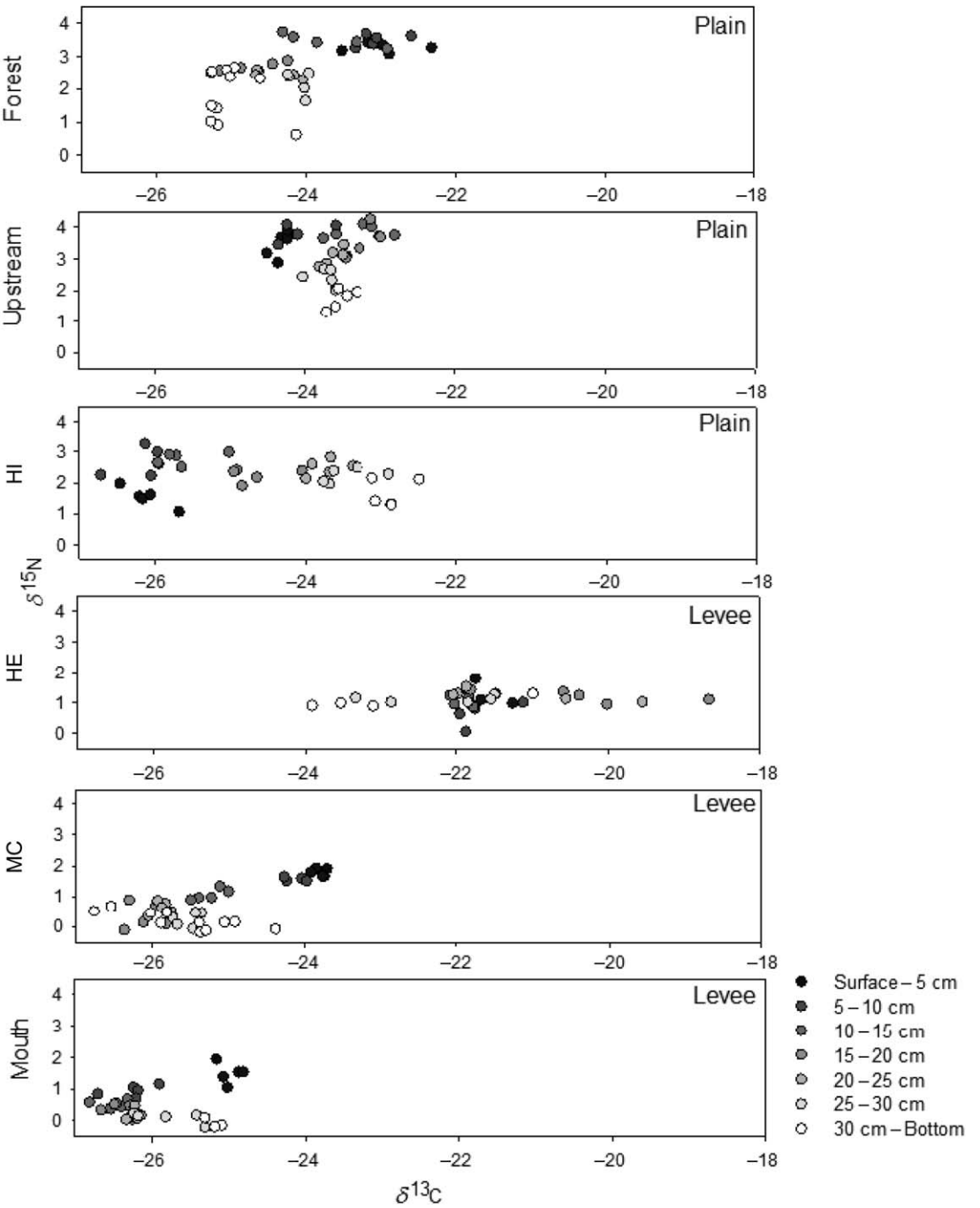

Fig. 3. δ^{15}N vs. δ^{13}C for all stations. Depth in the core is represented by gray scale with samples at the surface denoted by black circles. Overall, mouth and MC stations (Low Marsh) are the most depleted in δ^{13}C and δ^{15}N compared to the other sites, whereas the HE station has a more enriched δ^{13}C signature. The HI station displays variability that indicates blending of marine and terrestrial OM sources with depth.

of sediment deposited between the marsh levee and plain. Natural creek levees are exposed to more deposition of finer suspended particles in the water column because of the reduction of water velocity caused by fringing vegetation interference (Friedrichs and Perry 2001). Sediments composed of mixed, rather than homogenous, grain sizes have lower porosities because the smaller grains fill the void spaces between the larger (Fetter 2001) such as in the ancient sand dune ridges underlying the High Marsh. Due to the low regional gradient and lack of terrestrial sand supply (Hine et al. 1988), sediment for the lower reaches of the creek likely comes from mudflats and sand bars near the mouth.

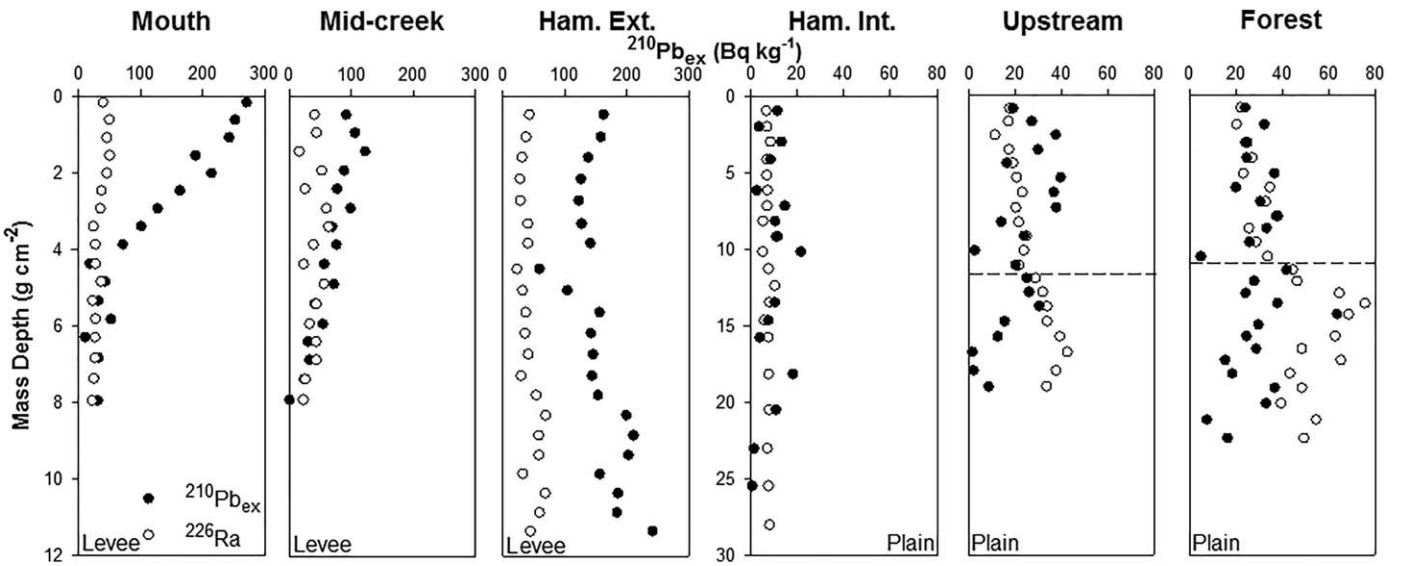

Fig. 4. Excess ^{210}Pb and the parent ^{226}Ra isotope (Bq kg^{-1}) vs. mass depth (g cm^{-2}) for each station. The Hammock stations appear to have mixed sediment profiles, therefore, neither core could be dated for accumulation and burial rates. Ra-226 at the upstream and forest stations increases below a mass depth around 13 g cm^{-2}, indicated by the dashed lines. Note: scale for mass depth is larger and the excess ^{210}Pb scale is smaller for the plain sites.

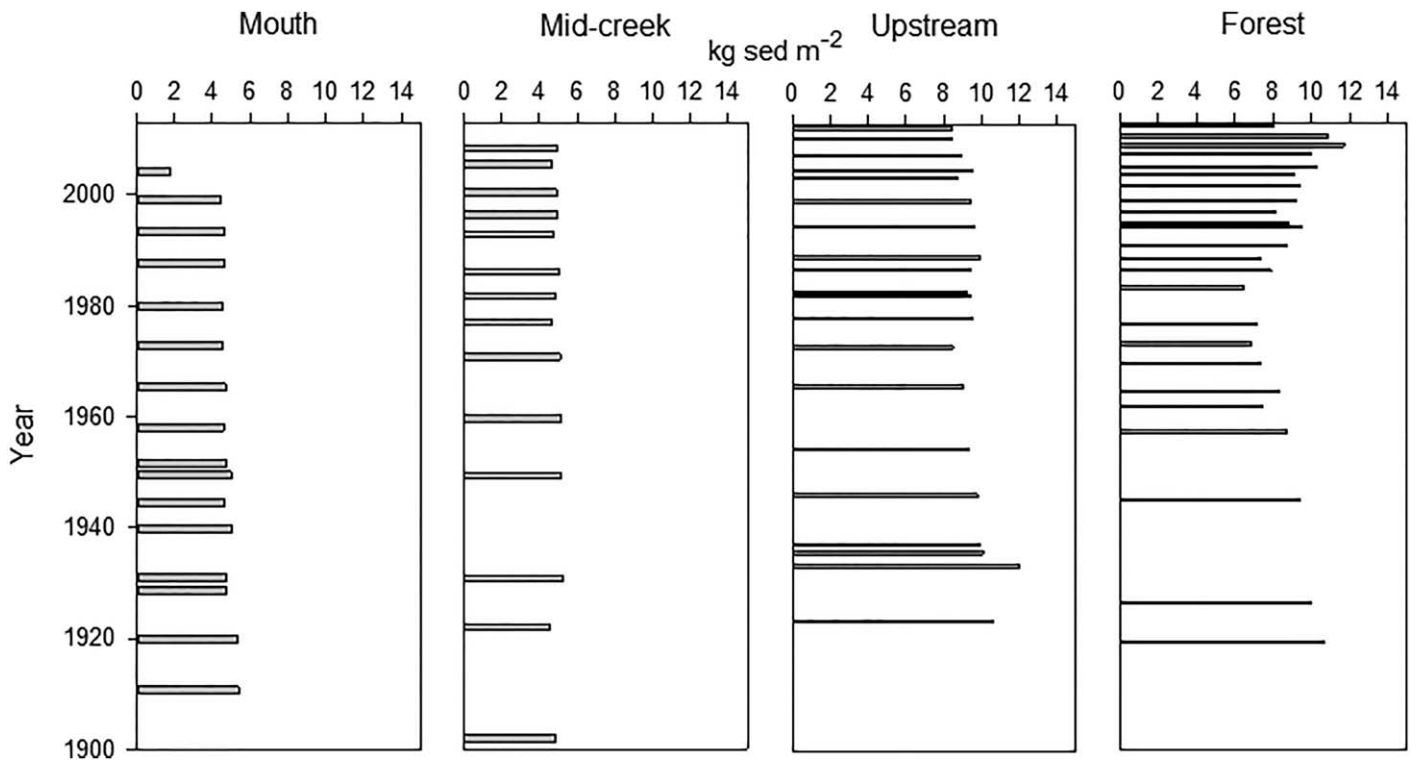

Fig. 5. Total mass inventory (kg$_{sed}$ m^{-2}) vs. year of deposition for Low and High Marsh stations. The least amount of accumulation is apparent in the Low Marsh of Snipe Creek and appears to increase moving upstream toward the headwaters from the mouth to the forest station. Values here are represented in kg, but are reported as g in the text and Supporting Information.

Marsh plains have been identified as having low accumulation of OM due to the decrease in sediment deposition from a lack of tidal inundation or a decrease in vegetation density (Kruczynski et al. 1978; Craft et al. 1993). However, the High Marsh and HI stations are almost devoid of sediment associated OM. A study on marsh zone plant

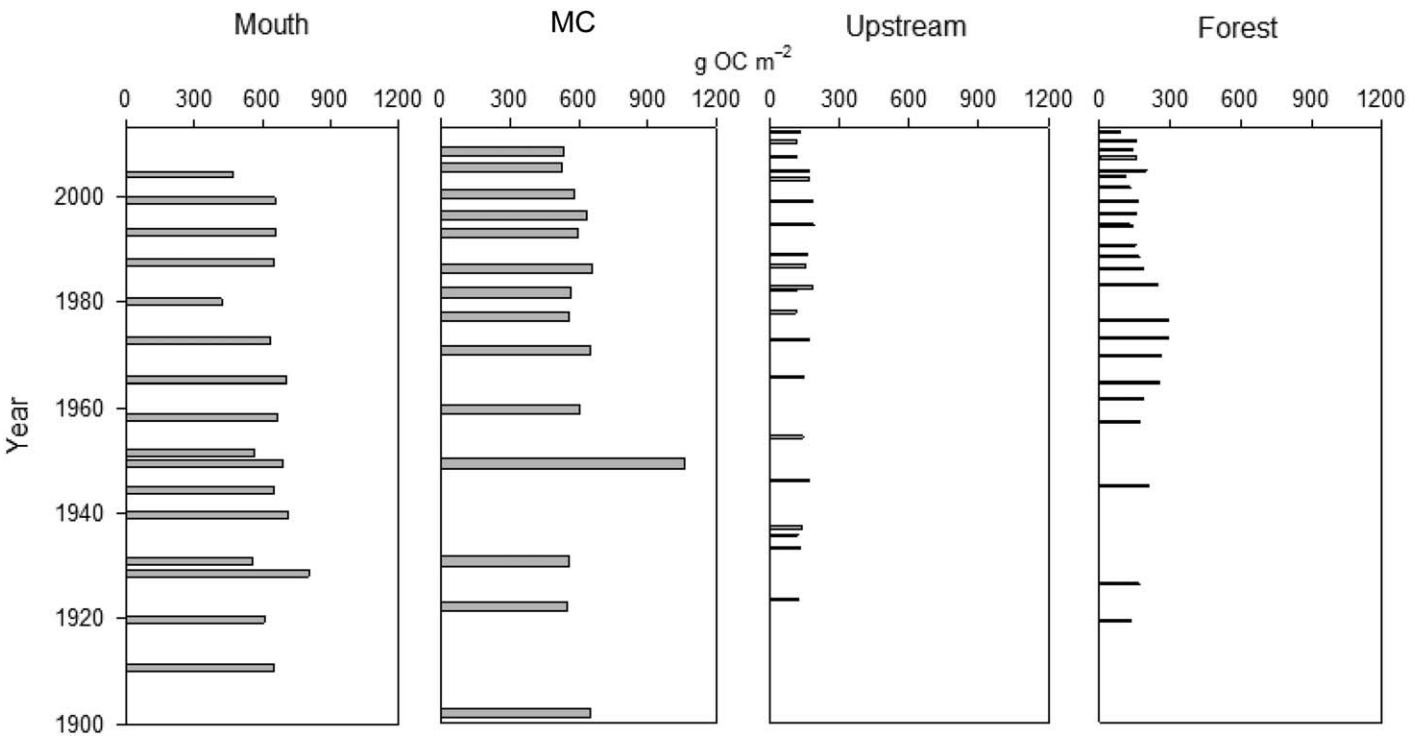

Fig. 6. Carbon inventory (g OC m^{-2}) vs. year of deposition for Low and High Marsh stations. The mouth and MC stations have the highest carbon inventory along this tidal creek with the lowest amounts seen near the headwaters.

community structure was performed within the St. Marks National Wildlife Refuge (Fig. 1a, Kruczynski et al. 1978) about 20 km northwest of Snipe Creek and found that, although root and rhizome underground biomass was generally higher, the total above ground production per hectare decreased with increasing distance from mean low water, resulting in less buried OM. This lower % OM resulted in a lower CBR of 44 g m^{-2} yr^{-1} at the St. Marks site (Chmura et al. 2003). They also found that mean total above ground biomass of *J. roemerianus* and *S. alterniflora* was highest in the low marsh and decreased with distance from mean low water (Kruczynski et al. 1978).

Sediment OM content and porosity are distinctly higher at the levee sites. The mean biomass density of *J. roemerianus* and *S. alterniflora* at Snipe Creek were estimated to be 544 ± 260 g dry weight (dw) m^{-2} and 1287 ± 488 g dw m^{-2}, respectively (D. Seminara and J. Schalles pers. comm.). In a study on marsh biota in Mississippi, *S. alterniflora* was found to have a lower mean annual production of $40.37\% \pm 1.01\%$ C dw, compared to *J. roemerianus* of $45.15\% \pm 0.72\%$ C dw (De La Cruz 1983). By multiplying the estimated mean dry weight for *J. roemerianus* and *S. alterniflora* determined for Snipe Creek by the % C dw gives a rough above ground C estimate of 246 g C m^{-2} and 520 g C m^{-2}, respectively. For this marsh, *S. alterniflora* has potentially twice the amount of C stored in above ground biomass than *J. roemerianus*, meaning the lower marsh and levee sites have a larger source of autochthonous C and OM due to the presence of *S. alterniflora* than the rest of the marsh.

Sources of organic material

The stable isotopes δ^{13}C and δ^{15}N were used to interpret the vegetation source contributing to the organic content within the sediment matrix (e.g., Haines 1976; Ember et al. 1987; Craft 1988; Middelburg et al. 1997; Choi et al. 2001; Wang et al. 2003). While the range in δ^{15}N values for all marsh sites is similar, the range of δ^{13}C values infers a change in OM sources along the tidal creek - salt marsh gradient. The δ^{13}C values of the Low Marsh range from -23.7‰ to -26.8‰ and reveals the vegetation source to be of a C3 photosynthetic pathway origin, which has a δ^{13}C extent of -20‰ to -34‰ (Craft 1988). *J. roemerianus*, the prevailing vegetation species in the Low Marsh, has a C3 pathway. Our results agree well with a study performed at the mouth of the St. Marks River, about 23 km northwest of Snipe Creek where *J. roemerianus* plant material from the marsh yielded a δ^{13}C of -27‰ (Choi et al. 2001).

The range of δ^{13}C values (-19‰ to -24‰) for the HI covers those of the Low and High Marsh, indicating the Hammock is a mixing site of varying OM sources. The dominant C4 pathway species along the marsh levee, *S. alterniflora*, typically has a δ^{13}C range of -6‰ to -19‰ (Craft 1988) and is a more prominent species at this station than *J. roemerianus*. Wang et al. (2003) reported δ^{13}C values ranging from

Table 1. Mean (± 1 σ) values for porosity, OM (%), TOC (g OC g_{sed}^{-1}), TN (g N g_{sed}^{-1}), $\delta^{13}C$, VAR (mm yr^{-1}), MAR (g_{sed} m^{-2} yr^{-1}), total mass accumulated (TMA; g_{sed} m^{-2}), CBR (g OC m^{-2} yr^{-1}), and total carbon accumulated (TCA; g OC m^{-2}) for all stations. N/A = data not available.

Station ID	Porosity	OM (%)	TOC (g OC g_{sed}^{-1})	TN (g N g_{sed}^{-1})	$\delta^{13}C$	VAR (mm yr^{-1})	MAR (g_{sed} m^{-2} yr^{-1})	TMA (g_{sed} m^{-2})	CBR (g OC m^{-2} yr^{-1})	TCA (g OC m^{-2})
Mouth	0.55 (0.07)	34.2 (11.7)	0.11 (0.02)	0.0076 (0.003)	−25.9 (0.6)	1.5 (0.5)	820.9 (229.2)	5148.5 (945.5)	109.5 (36.0)	583.9 (113.4)
MC	0.56 (0.04)	33.6 (7.4)	0.12 (0.02)	0.0077 (0.002)	−25.2 (0.9)	0.9 (0.9)	777.6 (449.3)	5151.2 (311.9)	95.7 (51.4)	624.3 (115.9)
HE	0.54 (0.06)	30.7 (7.4)	0.11 (0.04)	0.0079 (0.002)	−21.7 (1.1)	N/A	N/A	5265.0 (420.4)	N/A	561.0 (162.6)
HI	0.34 (0.03)	2.8 (1.5)	0.005 (0.002)	0.0004 (0.0001)	−24.7 (1.3)	N/A	N/A	11,708.1 (1283.0)	N/A	63.0 (13.3)
Upstream	0.36 (0.06)	5.6 (2.1)	0.013 (0.005)	0.0009 (0.0003)	−23.7 (0.5)	2.2 (1.8)	3245.7 (1850.2)	10,343.1 (1373.0)	49.5 (24.8)	126.8 (40.3)
Forest	0.35 (0.07)	6.9 (5.1)	0.015 (0.01)	0.0012 (0.0009)	−24.1 (0.9)	2.0 (2.1)	3563.1 (2166.8)	10,958.5 (2963.8)	65.2 (28.6)	134.7 (76.2)

−17.7‰ to −20.6‰ for a *S. alterniflora* dominated marsh on Plum Island, Massachusetts. The exterior Hammock $\delta^{13}C$ results cover most of the Plum Island range, but are still slightly more depleted. The $\delta^{13}C$ at the HE could be the results of a blending of C isotope contributions from *S. alterniflora*, *J. roemerianus*, and potentially other sources of carbon.

Vertical accretion and mass accumulation rates

The relative sea level rise (RSLR) estimate for the Big Bend region of Florida is 1.97 ± 0.18 mm yr^{-1} as derived from a 100-yr record of mean sea level in Cedar Key (*see* "Study site" section) (tidesandcurrents.noaa.gov). Compared to this RSLR estimate, the mean Low Marsh VAR of 1.2 ± 0.42 mm yr^{-1} is behind in keeping pace with RSLR. Thus, the Low Marsh is vulnerable to increasing inundation and eventual permanent submersion if either a decrease in sedimentation or an increase in the rate of RSLR occurs. The High Marsh site is slightly above RSLR at 2.1 ± 0.14 mm yr^{-1}. While the overall mean accretion rate of Snipe Creek marsh (1.65 ± 0.58 mm yr^{-1}) is slower than RSLR, the location along the creek in relation to the rate of RSLR will impact carbon storage.

A global review of accretion and CBRs in salt marshes revealed accretion rates range from 0.8 mm yr^{-1} to 35 mm yr^{-1} in the GoM (Ouyang and Lee 2014; Table 2). After including our accretion rate results from Snipe Creek, the mean rate of vertical accretion for the GoM is 7.8 ± 8.3 mm yr^{-1}. Snipe Creek is currently behind in keeping pace with RSLR, but relative to the GoM it is lagging by more than 6 mm yr^{-1}. However, using the mean of all the GoM studies is not a strong comparison for Snipe Creek vertical accretion because a variety of methods were used to determine these sediment accretion rates, including feldspar markers and ^{137}Cs, with integrations over variable time scales. Methods for calculating TOC also varied in these studies and were dominantly determined using bulk organic material conversions to OC content instead of direct measurement. Utilizing the same accretion and TOC assessment methods across studies would give robustness to a future regional vertical accretion comparison.

The total sediment mass accumulated for the entire core for the mouth, MC, HE, HI, upstream, and near forest stations are 17.0×10^4 g m^{-2}, 21.1×10^4 g m^{-2}, 17.9×10^4 g m^{-2}, 41.0×10^4 g m^{-2}, 36.2×10^4 g m^{-2}, and 43.8×10^4 g m^{-2}, respectively (Fig. 7a). The Hammock site accumulations represent a site minimum since we were unable to date these cores due to in situ sediment mixing, but it does provide an overall sediment inventory. This figure emphasizes the scope of mass accumulation variability in this marsh, where total accumulated mass in the plain sites (HI, S, and F) is two times higher than the levee sites (M, MC, and HE). The primary sediment source for the levee is likely fine particles from the surrounding marsh or adjacent mudflats because the flat slope of the landscape prevents transport of modern

Table 2. Accretion and CBRs from studies around the GoM. RSLR rates are based on the nearest NOAA water level gauge (tidesandcurrents.noaa.gov). Net accretion rates are calculated as accretion rate minus RSLR rate. The ranges of accretion and CBRs from this study (Snipe Creek, FL) are listed for comparison at the bottom. Adapted from Ouyang and Lee (2014). N/A = data not available.

Site	Marsh type	Accretion rate (mm yr^{-1})	RSLR (mm yr^{-1})	Net accretion rate (mm yr^{-1})	CBR (g C m^{-2} yr^{-1})	Source
Aransas, TX	*S. alterniflora*, *Salicornia virginica*	4.5	5.33	−0.83	178.0	1
San Bernard, TX	*S. alterniflora*, *Batis maritima*	6.2	4.43	1.77	203.0	1
McFaddin NWR, TX	*N/A*	7.9	6.62	1.28	95.0	2
Sabine NWR, LA	*N/A*	5.9–9.0	5.54	0.36–3.46	714.0–1713.0	3
Cameron Parish, LA	*N/A*	4.3–11.3*	9.65	−5.35 to 1.65	41.0–115.0	4
Rockefeller Refuge, LA	*Spartina patens*	0.8–11.0	9.65	−8.85 to 1.35	27.0–448.0	5
Rockefeller Refuge, LA	*N/A*	2.9–5.5	9.65	−6.75 to −4.15	349.0–657.0	3
Marsh Island, LA	*N/A*	2.9–7.0	9.65	−6.75 to −2.65	318.0–763.0	3
Old Oyster Bayou, LA	*S. alterniflora*	28.5	9.05	19.45	602.6	6
Old Oyster Bayou, LA	*N/A*	4.4	9.05	−4.65	84.0	2
Fina la-Terre, LA	*S. patens*	1.0–5.0	9.05	−8.05 to −4.05	18.0–136.0	5
Bayou Chitigue, LA	*S. alterniflora*	35.0	9.05	25.95	669.0	6
Bayou Chitigue, LA	*N/A*	32.3	9.05	23.25	516.0	2
Lafourche Parish, LA	*N/A*	9.9	9.05	0.85	186.0	4
Barataria Basin, LA	*S. alterniflora*, *S. patens*, *J. roemerianus*	3.8–16.9	9.05	−5.25 to 7.85	71.0–185.0	2,7
Three Bayous, LA	*N/A*	8.3	9.05	−0.75	116.0	2
St. Bernard Parish, LA	*S. patens*	5.0	9.05	−4.05	140.0†	8
Biloxi Bay, MS	*J. roemerianus*, *S. alterniflora*	5.7	4.10	1.6	153.0	1
St. Marks, FL	*N/A*	1.8	1.96	−0.16	44.0	2
Snipe Creek, FL	*J. roemerianus*, *S. alterniflora*	*0.9–2.2**	*1.97*	*−1.07 to 0.23*	*49.5–109.5†*	9
Mean (± 1 σ)		**7.8 (8.3)**	**7.8 (2.4)**	**2.24 (9.32)**	**290.8 (333.4)**	
Median		5.5	9.05	−0.29	153.0	

1. Callaway et al. (1997); 2. Chmura et al. (2003); 3. Bryant and Chabreck (1998); 4. Cahoon and Turner (1989); 5. Cahoon (1994); 6. Day et al. (2011); 7. Hatton et al. (1983); 8. Markewich (1998); 9. This study.
* ^{210}Pb measurement.
† Based on direct TOC measurements.

or relict sediment downstream from the coastal forest and ancient sand dunes. It is not surprising that the highest continuous total mass sedimentation rates are found further inland.

CBRs

The range of CBRs in salt marshes along the GoM is essentially the same as worldwide averages, 18–1713 g C m^{-2} yr^{-1}, with a mean burial rate of 290.8 ± 333.4 g C m^{-2} yr^{-1} including the results from Snipe Creek (Ouyang and Lee 2014; Table 2). By summing the carbon buried for the entire core, the total amount of carbon stored at the mouth, MC, HE, HI, upstream, and forest stations are 19.3 × 10^3 g OC m^{-2}, 25.6 × 10^3 g OC m^{-2}, 19.1 × 10^3 g OC m^{-2}, 2.20 × 10^3 g OC m^{-2}, 4.44 × 10^3 g OC m^{-2}, and 5.39 × 10^3 g OC m^{-2}, respectively (Fig. 7b). Unlike total mass accumulation, the highest concentration of TOC is buried in the levee, whereas the least is in the plain sites. Low tidal flushing in the plain should result in most of the plant material remaining in the marsh as wrack (Craft et al. 1993), yet this detritus does not appear to remain at this site because of the minimal % OM and TOC concentrations. Higher sediment deposition, as evident in the total mass accumulation rates, could be diluting the autochthonous OM and subsequent sediment TOC in the plain sites. Another possibility is a reduction in above ground vegetation biomass production in the High Marsh zone which was observed in the nearby St. Marks salt marsh (Kruczynski et al. 1978).

Total mass accumulation and CBRs can vary by orders of magnitude even within short distances along a creek system.

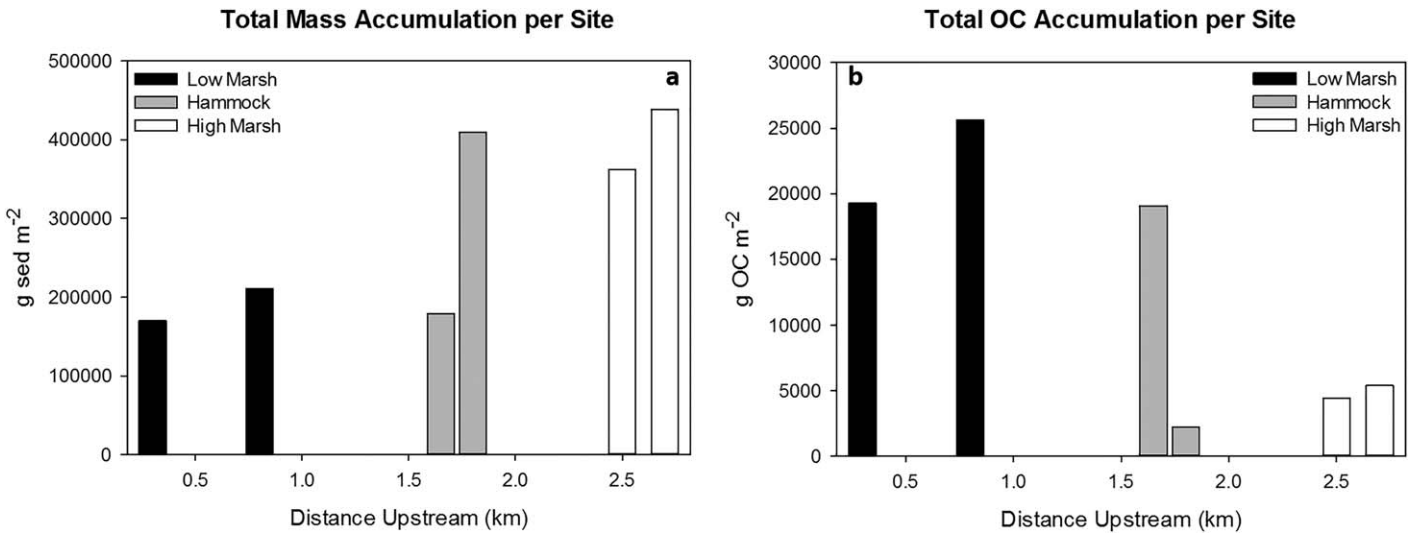

Fig. 7. (**a**) Total mass accumulation stocks (g_{sed} m^{-2}) at each station with distance (km) from the mouth along the *x*-axis. The Low Marsh (black bars) and HE (gray bar at 1.6 km) display the lowest total mass accumulation with the highest values in the HI (gray bar at 1.8 km) and the High Marsh (white bars). (**b**) Total carbon accumulation stocks (g OC m^{-2}) at each station with distance from the mouth along the *x*-axis. The highest values are now found at the Low Marsh and the lowest are in the High Marsh. Hammock marsh values represent an estimate since we were unable to date this site using $^{210}Pb_{ex}$, but still provides an overall stock.

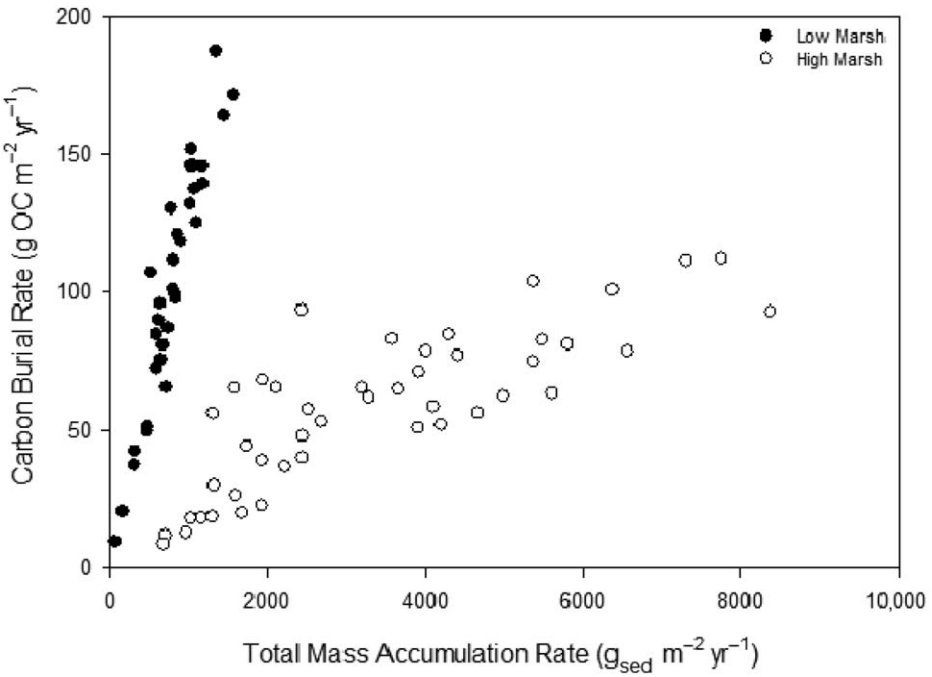

Fig. 8. The Low Marsh site (closed circles) have the highest rates of carbon burial (g OC m^{-2} yr^{-1}), but the lowest total mass accumulation rates (g_{sed} m^{-2} yr^{-1}). Converse to this trend, the High Marsh (open circles) has lower CBRs, but higher rates of total mass accumulation.

Similar to Callaway et al. (1997) in the GoM, the spatial variability in the carbon burial potential of this system is easily observed when compared directly to total sediment mass accumulation rates (Fig. 8). The Low and High Marsh along Snipe Creek display strong linear relationships between carbon burial and mass accumulation rates. Additionally, two trends occur at the end members of this system, where a bifurcation occurs between sediment and carbon accumulation from Low to High Marsh. In the Low Marsh, we observe high CBRs with low sedimentation, while the High Marsh

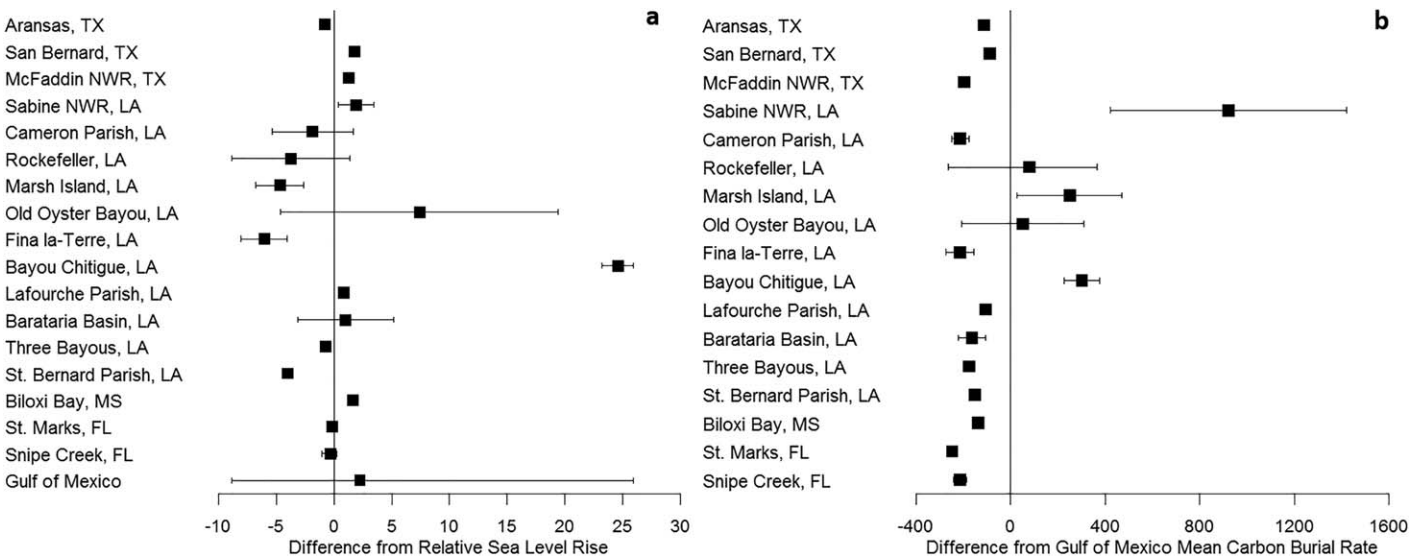

Fig. 9. (**a**) Forest plot illustrating the mean (black boxes) and ranges of the difference from the relative mean sea level (mm yr^{-1}), or net VARs, per GoM site using data from Table 2. (**b**) Forest plot of the mean (black boxes) and ranges of the difference of CBRs (g OC m^{-2} yr^{-1}) from each study site compared to the GoM mean CBR based on data from Table 2.

demonstrates the opposite trend of low CBRs with high sedimentation dominating. Previous studies have shown that sediment deposition is typically higher in the lower marsh, resulting in higher carbon accumulation (Chmura et al. 2003). However, here the Low Marsh has the slowest VARs in the system, but contains the relatively higher CBRs in this marsh (Fig. 8). The higher rates of carbon burial in the Low Marsh, but vertical accretion is lagging behind current rates of RSLR, implies that the carbon stored in this site is the most vulnerable to increasing rates of SLR.

Regional implications

The net vertical accretion (sediment VAR minus the rate of RSLR) determines the vulnerability of a marsh to SLR. Figure 9a illustrates the ranges and means of net vertical accretion per site and overall for the GoM. A marsh is considered keeping pace with SLR the closer the accretion rate is to RSLR and is considered vulnerable when the marsh has a negative net accretion rate. The mean net accretion for Snipe Creek is −0.32 mm yr^{-1}, whereas the mean net accretion rate for the GoM overall is 2.24 mm yr^{-1}, but the GoM mean is skewed by an extremely high accretion rate at Bayou Chitigue, LA (Fig. 9a).

As with Snipe Creek, CBRs need to also be considered when predicting GoM marsh vulnerability in the face of SLR. Salt marshes can have low net accretion rates, but high carbon burial if there is an abundance of sediment associated OM. Using the mean GoM CBR of 290.8 g OC m^{-2} yr^{-1} as a target, GoM CBR means and ranges are plotted in Fig. 9b. Marshes that have CBRs higher than the mean GoM rate, but also have negative net accretion rates, are critically vulnerable to SLR. When comparing Fig. 9a,b, Rockefeller and Marsh Island, LA, are sites that have negative mean net accretion rates, but higher mean CBRs. The loss of these two marshes to inundation and erosion via SLR means degradation of valuable carbon storage and the potential release of CO_2 back to the atmosphere.

Sediment associated carbon is not the only potential carbon storage in this region threatened in the face of SLR. We should not only be concerned with what happens to the buried carbon with increasing inundation, but also changes in the aboveground carbon stock that occurs with ecosystem conversion, such as landward marsh migration, with increasing rates of SLR. The uncertainty of whether coastal forest will be taken over by marsh vegetation or open water remains. Saltwater intrusion of groundwater is a prominent threat in coastal areas. Field et al. (2016) found that New England coastal forests showed resilience to marsh landward migration over a 10 yr period where they observed decreases in high marsh vegetation and increases in more flood tolerant marsh species with increased coastal inundation. They predict, however, that stress from increased saltwater inundation will reach a tipping point, followed by rapid and widespread tree mortality (Field et al. 2016). As groundwater salinity increases, forest vegetation will reduce water consumption which can lead to death and eventual replacement by marsh vegetation or open water (Craft 2012). This ecosystem conversion process has already begun, as evident in the surviving tree hammocks, along the Big Bend of Florida and may continue inland with increasing rates of SLR.

Conclusions

- The average VAR of Snipe Creek salt marsh is 1.65 mm yr^{-1} which is lagging behind the RSLR rate of 1.97 mm yr^{-1}.

- The Low Marsh has the highest carbon burial, but this site is also the most susceptible to erosion and conversion to open water due to increasing rates of SLR and slow VARs.
- Two trends exist at the end members of this tidal creek resulting in a bifurcation between sediment and carbon accumulation from Low to High Marsh.
- The average net VAR for the GoM is only 2.24 mm yr^{-1}, however, this value is skewed due to high accretion rates in Bayou Chitigue, LA, therefore marshes in this region are extremely vulnerable to inundation via SLR and the eventual loss of carbon storage.

References

Appleby, P. G., and F. Oldfield. 1978. The calculation of lead-210 dates assuming a constant rate of supply of unsupported 210 Pb to the sediment. Catena **5**: 1–8. doi:10.1016/S0341-8162(78)80002-2

Appleby, P. G., and F. Oldfield. 1983. The assessment of 210Pb data from sites with varying sedimentation rates. Hydrobiologia **103**: 29–35. doi:10.1007/BF00028424

Bala, G. 2013. Digesting 400 ppm for global mean CO2 concentration. Curr. Sci. **104**: 1471–1471.

Bost, M. C. 2016. How storms affect carbon burial in the New River Estuary, North Carolina. Master's thesis. Univ. of North Carolina at Chapel Hill.

Bryant, J. C., and R. H. Chabreck. 1998. Effects of impoundment on vertical accretion of coastal marsh. Estuaries **21**: 416–422. doi:10.2307/1352840

Burnett, W. C., J. B. Cowart, and S. Deetae. 1990. Radium in the Suwannee River and estuary. Biogeochemistry **10**: 237–255. doi:10.1007/BF00003146

Cahoon, D. R. 1994. Recent accretion in two managed marsh impoundments in coastal Louisiana. Ecol. Appl. **4**: 166–176. doi:10.2307/1942126

Cahoon, D. R., and R. E. Turner. 1989. Accretion and canal impacts in a rapidly subsiding wetland II. Feldspar marker horizon technique. Estuaries Coast. **12**: 260–268. doi:10.2307/1351905

Cahoon, D. R., D. J. Reed, and J. W. Day. 1995. Estimating shallow subsidence in microtidal salt marshes of the southeastern United States: Kaye and Barghoorn revisited. Mar. Geol. **128**: 1–9. doi:10.1016/0025-3227(95)00087-F

Callaway, J. C., R. D. DeLaune, and W. H. Patrick, Jr. 1997. Sediment accretion rates from four coastal wetlands along the Gulf of Mexico. J. Coast. Res. **13**: 181–191. doi:10.1016/s12237-012-9508-9

Callaway, J. C., E. L. Borgnis, R. E. Turner, and C. S. Milan. 2012. Carbon sequestration and sediment accretion in San Francisco Bay tidal wetlands. Estuaries Coast. **35**: 1163–1181. doi:10.1007/s12237-012-9508-9

Chmura, G. L. 2013. What do we need to assess the sustainability of the tidal salt marsh carbon sink? Ocean Coast. Manag. **83**: 25–31. doi:10.1016/j.ocecoaman.2011.09.006

Chmura, G. L., S. C. Anisfeld, D. R. Cahoon, and J. C. Lynch. 2003. Global carbon sequestration in tidal, saline wetland soils. Global Biogeochem. Cycles **17**: 1111–1123. doi:10.1029/2002GB001917

Choi, Y., Y. Wang, Y. P. Hsieh, and L. Robinson. 2001. Vegetation succession and carbon sequestration in a coastal wetland in northwest Florida: Evidence from carbon isotopes. Global Biogeochem. Cycles **15**: 311–319. doi:10.1029/2000GB001308

Corbett, D. R., K. Dillon, W. Burnett, and J. Chanton. 2000. Estimating the groundwater contribution into Florida Bay via natural tracers, ^{222}Rn and CH_4. Limnol. Oceanogr. **45**: 1546–1557. doi:10.4319/lo.2000.45.7.1546

Coultas, C. L. 1980. Soils of marshes in the Apalachicola, Florida estuary. Soil Sci. Soc. Am. J. **44**: 348–353. doi:10.2136/sssaj1980.03615995004400020028x

Coultas, C. L., and E. R. Gross. 1975. Distribution and properties of some tidal marsh soils of Apalachee Bay, Florida. Soil Sci. Soc. Am. J. **39**: 914–919. doi:10.2136/sssaj1975.03615995003900050034x

Craft, C. B. 2012. Tidal freshwater forest accretion does not keep pace with sea level rise. Glob. Chang. Biol. **18**: 3615–3623. doi:10.1111/gcb.12009

Craft, C. B., Seneca, E.D., and Broome, S.W. 1993. Vertical accretion in microtidal regularly and irregularly flooded estuarine marshes. Estuarine, Coastal and Shelf Science **37**: 371–386. doi:10.1006/ecss.1993.1062

Day, J. W., G. P. Kemp, D. J. Reed, D. R. Cahoon, R. M. Boumans, J. M. Suhayda, and R. Gambrell. 2011. Vegetation death and rapid loss of surface elevation in two contrasting Mississippi delta salt marshes: The role of sedimentation, autocompaction and sea-level rise. Ecol. Eng. **37**: 229–240. doi:10.1016/j.ecoleng.2010.11.021

De La Cruz, A. A. 1983. Caloric values of marsh biota, p. 1–32. Pub1. No. MASGP-83-006. Mississippi-Alabama Sea Grant Consortium.

Dingman, S. L. 2002. Physical hydrology, 2nd ed. Prentice-Hall.

Doney, S. C., V. J. Fabry, R. A. Feely, and J. A. Kleypas. 2009. Ocean acidification: The other CO_2 problem. Ann. Rev. Mar. Sci. **1**: 169–192. doi:10.1146/annurev.marine. 010908.163834

Ember, L. M., Williams, D. F., and Morris, J. T. 1987. Processes that influence carbon isotope variations in salt marsh sediments. Marine Ecology Progress Series **36**: 33–42. http://www.jstor.org/stable/24821250

Fetter, C. W. 2001. Applied hydrogeology, 4th ed. Prentice-Hall.

Field, C. R., C. Gjerdrum, and C. S. Elphick. 2016. Forest resistance to sea-level rise prevents landward migration of tidal marsh. Biological Conservation **201**: 363–369. doi:10.1016/j.biocon.2016.07.035

Friedrichs, C. T., and J. E. Perry. 2001. Tidal salt marsh morphodynamics: A synthesis. J. Coast. Res. **27**: 7–37. http://www.jstor.org/stable/25736162

Grubbs, J. W. 1998. Recharge rates to the Upper Floridan aquifer in the Suwannee River Water Management District, Florida (No. 97-4283). US Dept. of the Interior, US Geological Survey, USGS Information Services [distributor].

Haines, E. B. 1976. Stable carbon isotope ratios in the biota, soils and tidal water of a Georgia salt marsh. Estuarine and Coastal Marine Science **4**: 609–616. doi:10.1016/0302-3524(76)90069-4

Hatton, R. S., R. D. DeLaune, and W. E. I. Patrick, Jr. 1983. Sedimentation, accretion, and subsidence in marshes of Barataria Basin, Louisiana. Limnol. Oceanogr. **28**: 494–502. doi:10.4319/lo.1983.28.3.0494

Hine, A. C., D. F. Belknap, J. G. Hutton, E. B. Osking, and M. W. Evans. 1988. Recent geological history and modern sedimentary processes along an incipient, low-energy, epicontinental-sea coastline: northwest Florida. Journal of Sedimentary Research **58**: 567–579.

Hopkinson, C. S., W. J. Cai, and X. Hu. 2012. Carbon sequestration in wetland dominated coastal systems — a global sink of rapidly diminishing magnitude. Curr. Opin. Environ. Sustain. **4**: 186–194. doi:10.1016/j.cosust.2012.03.005

Houghton, R. A. 2003. The contemporary carbon cycle, p. 473–513. *In* H. D. Holland and K. K. Turekian [eds.], Treatise on geochemistry. Elsevier.

IPCC. 2014. Climate change 2014: Synthesis report. In Contribution of Working Groups I, II and III to the Fifth Assessment Report of the Intergovernmental Panel on Climate Change. [Core Writing Team, R. K. Pachauri, and L. A. Meyer [eds.]

Kruczynski, W. L., C. B. Subrahmanyam, and S. H. Drake. 1978. Studies on the plant community of a North Florida salt marsh part I. Primary production. Bull. Mar. Sci. **28**: 316–334.

Markewich, H. W. 1998. Carbon storage and late holocene chronos- tratigraphy of a Mississippi River deltaic marsh, St. Bernard Parish, Louisiana. Open-File Report 98– 36. US Geological Survey.

Mcleod, E., G. L. Chmura, S. Bouillon, R. Salm, M. Björk, C. M. Duarte, and B. R. Silliman. 2011. A blueprint for blue carbon: Toward an improved understanding of the role of vegetated coastal habitats in sequestering CO2. Front. Ecol. Environ. **9**: 552–560. doi:10.1890/110004

Meanley, B. 1965. Early-fall food and habitat of the sora in the Patuxtent River Marsh, Maryland. Chesapeake Sci. **6**: 235–237. doi:10.2307/1350821

Middelburg, J. J., J. Nieuwenhuize, R. K. Lubberts, and O. Van de Plassche. 1997. Organic carbon isotope systematics of coastal marshes. Estuarine, Coastal and Shelf Science **45**: 681–687. doi:10.1006/ecss.1997.0247

Montague, C., and H. Odum. 1997. Settings and functions, p. 9–33. *In* T. Bianchi, J. Pennock, and R. Twilley [eds.], Ecology and management of tidal marshes. St. Lucie Press.

Morris, J. T., P. V. Sundareshwar, C. T. Nietch, B. Kjerfve, and D. R. Cahoon. 2002. Responses of coastal wetlands to rising sea level. Ecology **83**: 2869–2877. doi:10.1890/0012-9658(2002)083[2869:ROCWTR]2.0.CO;2]

Morris, J. T., and others. 2016. Contributions of organic and inorganic matter to sediment volume and accretion in tidal wetlands at steady state. Earths Future **4**: 110–121. doi:10.1002/2015EF000334

Ouyang, X., and S. Y. Lee. 2014. Updated estimates of carbon accumulation rates in coastal marsh sediments. Biogeosciences **11**: 5057–5071. doi:10.5194/bg-11-5057-2014

Sanchez-Cabeza, J. A., and A. C. Ruiz-Fernandez. 2011. ^{210}Pb sediment radiochronology: An integrated formulation and classification of dating models. Geochim. Cosmochim. Acta **82**: 183–200. doi:10.1016/j.gca.2010.12.024

Wang, X. C., R. F. Chen, and A. Berry. 2003. Sources and preservation of organic matter in Plum Island salt marsh sediments (MA, USA): long-chain n-alkanes and stable carbon isotope compositions. Estuarine, Coastal and Shelf Science **58**: 917–928. doi:10.1016/j.ecss.2003.07.006

Williams, K., K. C. Ewel, R. P. Stumpf, F. E. Putz, and T. W. Workman. 1999. Sea-level rise and coastal forest retreat on the west coast of Florida, USA. Ecology **80**: 2045–2063. doi:10.1890/0012-9658(1999)080[2045:SLRACF]2.0.CO;2

Acknowledgments

We would like to thank Captain Gary Mears, Molly Bost, Drew Seminara, John Schalles, Gabrielle Lyons, and Kim Marsh for their assistance in the field, Rachel Housego for lab assistance, Brittany Jenner for LiDAR data interpretation, and the University of North Carolina at Chapel Hill. We would also like to thank Brent McKee and two anonymous reviewers for providing valuable comments and feedback on this paper. Sediment elemental analyses were performed at the Florida State University National High Magnetic Field Laboratory in Tallahassee, Florida, U.S.A. This project was funded by the NSF grant OCE-0928162.

Conflict of Interest

None declared.

Submitted 04 November 2016
Revised 05 April 2017; 12 July 2017
Accepted 13 July 2017

Associate editor: M. Dileep Kumar